Observation and Coupling of Domains in a Spin-Spiral Multiferroic

D. Meier,[1] M. Maringer,[1] Th. Lottermoser,[1] P. Becker,[2] L. Bohatý,[2] and M. Fiebig[1,*]

[1]*HISKP, Universität Bonn, Nussallee 14-16, 53115 Bonn, Germany*

[2]*Institut für Kristallographie, Universität zu Köln, Zülpicher Straße 49b, 50674 Köln, Germany*

(Received 5 October 2008; published 11 March 2009)

The coexistence, coupling, and manipulation of magnetic spiral domains and magnetically induced ferroelectric domains are spatially resolved by optical second harmonic generation in multiferroic $MnWO_4$. Eight types of magnetic domains couple to two ferroelectric domains. An electric field uniquely creates a magnetic single-domain state. A magnetic field quenches the spontaneous polarization while retaining its magnetic origin so that the ferroelectric domains are concealed instead of destroyed.

DOI: 10.1103/PhysRevLett.102.107202 PACS numbers: 75.60.Ch, 77.80.Dj, 77.80.Fm, 42.65.Ky

In the quest for novel multifunctional spintronics devices manipulation of magnetic properties by electric fields (and the reverse) is an important challenge. Materials with a coexistence of magnetic and ferroelectric order, called multiferroics, display a particularly rich variety of magnetoelectric cross-coupling phenomena [1–7]. The strongest interactions were discovered in compounds where a spontaneous electric polarization forms as a direct consequence of magnetic spiral order [8]. In spite of the tremendous interest in these compounds essential aspects of their ferroicity continue to be a mystery. Neither magnetic nor electric domains have been resolved in spin-spiral multiferroics thus far. Yet any magnetoelectric interaction between their sublattice magnetization or polarization and an external electric or magnetic field inevitably roots in coupling between the magnetic and electric domains.

Here we show how in view of the magnetic origin of the spontaneous polarization ferroelectric 180° domains are formed. Optical second harmonic generation (SHG) is used to resolve the magnetically induced ferroelectric domains in relation to the coexisting magnetic spin-spiral domains in $MnWO_4$. An electric field uniquely controls the magnetic domains. In addition, a magnetic field controls the poling behavior of the ferroelectric domains. It quenches the spontaneous polarization but not its magnetic origin so that the ferroelectrically stored information is concealed but not destroyed. Our observations substantially advance the concept of multiferroics with magnetically induced ferroelectricity and their application potential.

In general, long-range order reduces the symmetry of a crystal. For instance, exchanging the spatial coordinate $\vec{r}$ with $-\vec{r}$ reverses the electric dipole moment so that ferroelectric (FEL) order, which is characterized by the formation of a spontaneous electric polarization, violates the inversion symmetry. Recently, it was discovered that, if a magnetically ordered state violates the spatial inversion symmetry, this can be accompanied by the formation of a spontaneous electric polarization. This is the case in magnetic spiral structures and described by the equation [8,9]

$$\vec{P} \propto \vec{e}_{ij} \times (\vec{S}_i \times \vec{S}_j), \tag{1}$$

where $\vec{S}_{i,j}$ denotes spins at neighboring sites i and j connected by the unit vector $\vec{e}_{ij}$. The double vector product transforms like an electric polarization and connects magnetic spiral order to FEL order. Among the spin-spiral multiferroics $MnWO_4$ is an outstanding compound. With only a transition-metal ion contributing to magnetic order, its structure is relatively simple but nevertheless has great flexibility for displaying magnetoelectric coupling effects because of the complexity of the Mn^{2+} spin spiral [10,11].

$MnWO_4$ displays commensurate collinear antiferromagnetic (AFM) order at $T < 7.6$ K (AF1 phase), incommensurate noncollinear AFM order at $7.6\ \mathrm{K} < T < 12.7$ K (AF2 phase), and incommensurate collinear AFM order at $12.7\ \mathrm{K} < T < 13.5$ K (AF3 phase). The AF2 phase with a magnetic spiral characterized by the propagation vector $\vec{k} = (-0.214, \frac{1}{2}, 0.457)$ [10] is multiferroic with a polarization density of up to 57 $\mu\mathrm{C/m}^{-2}$ [11,12]. The crystallographic point symmetry in the paramagnetic state is $2/m1'$ (Cartesian coordinates x, y, z here replace a, b, c of the monoclinic crystal since $\beta = 91.1° \approx 90°$). The FEL polarization reduces the crystallographic symmetry to $21'$ with two FEL 180° domains of polarization $\pm P_y$. The magnetic symmetry is even lower because 2, m, and $1'$ are no longer symmetry operations. The broken symmetry operations lead to domains. Application of m leads to two so-called K domains which can be attributed to the magnetic propagation vectors $\vec{k}_1 = (k_x, \pm\frac{1}{2}, k_z)$ and $\vec{k}_2 = (-k_x, \pm\frac{1}{2}, -k_z)$. These k vectors are identical in the AF3 and the AF2 phases [10,13]. In the AF2 phase $+k_{x,z}$ and $-k_{x,z}$ are associated to a left-handed ($P_y < 0$) and a right-handed ($P_y > 0$) spin spiral, respectively, with a spontaneous polarization as in Eq. (1). Application of $1'$ leads to two 180° domains for the spin spiral that are characterized by a reversal of all spins upon crossing the domain wall. Application of 2 leads to two types of rotation domains distinguished by a reversal of the x and z components of each Mn^{2+} spin in the spiral upon crossing the domain

wall. The K domains of the AF2 phase differ in an absolute way (i.e., their chirality), while the 180° domains and the rotation domains are mere translation domains: a 180°- or rotation-domain wall corresponds to different types of three-dimensional shifts of the spin lattice by less than a period of the incommensurate spin cycloid. In total, eight types of AFM domains are expected: two sets of domains with opposite chirality, each composed of four types of translation domains [10,14].

A powerful method for imaging (anti)ferroic domain structures is optical SHG [15,16]. An electromagnetic light field $\vec{E}$ at frequency ω is incident on a crystal, inducing an electric or magnetic dipole oscillation at frequency 2ω, which acts as a source $\vec{S}(2\omega)$ of a frequency-doubled light wave. This is expressed by $\vec{S}(2\omega) = \varepsilon_0 \hat{\chi}\, \vec{E}(\omega)\vec{E}(\omega)$ with $\hat{\chi}$ as SHG susceptibility and $I(2\omega) \propto |\vec{S}|^2 \propto |\vec{E}(\omega)|^4$ as intensity of the emitted SHG wave. Following the Neumann principle, symmetry determines the set of tensor components $\chi_{ijk} \neq 0$. Long-range ordering affects the symmetry. This leads to contributions $\propto \hat{\chi}(\mathcal{O})$ to SHG which differ in amplitude and/or phase depending on the orientation of the order parameter $\mathcal{O}$, thus allowing one to distinguish domains. Since each form of (anti)ferroic order affects symmetry in a different way, the SHG contributions from $\hat{\chi}(\mathcal{O}_1)$, $\hat{\chi}(\mathcal{O}_2)$, etc., in a multiferroic are in general differently polarized. It is thus possible to image even coexisting magnetic and FEL domain structures separately by polarization analysis of the SHG signal [17].

SHG data were obtained on polished $MnWO_4$ samples with a thickness of 60 or 830 μm using an experimental setup described elsewhere [16]. Figure 1 shows the spectral and temperature dependence of two contributions to the SHG signal. SHG from χ_{yzz} corresponds to y-polarized SHG light obtained from z-polarized incident light. SHG from χ_{mix} combines contributions from several components χ_{ijk} because the incident fundamental and the emitted SHG light were chosen to include x-, y-, and z-polarized contributions. Figure 1 reveals three fundamentally different types of SHG: (i) A contribution χ_{para} already present in the paramagnetic phase. It couples to the crystallographic structure only but to none of the (anti) ferroic phases. It is the only contribution present above 13.5 K and mixes with other contributions below 13.5 K. (ii) A contribution χ_{FEL} coupling to the magnetically induced FEL polarization. This is the contribution constituting χ_{yzz} because $\chi_{yzz} \neq 0$ is obtained in the multiferroic AF2 phase only and its temperature dependence exactly reproduces the temperature dependence of the spontaneous polarization [12] in Fig. 1. Emergence of χ_{yzz} is compatible with the reduction of the crystallographic symmetry $(2/m1' \rightarrow 21')$ by the FEL polarization [18]. (iii) A contribution χ_{AFM} coupling to the AFM order. This contribution is present in χ_{mix} below 13.5 K where it interferes with the paramagnetic contribution χ_{para}. Its magnetic origin is evidenced by its sensitivity to the magnetic phase transitions and a temperature dependence different from that of χ_{FEL}. Note that the direction and polarization of the incident light were chosen such that FEL contributions to χ_{mix} are suppressed in favor of AFM contributions χ_{ijk} that are allowed for a symmetry lower than $21'$ only.

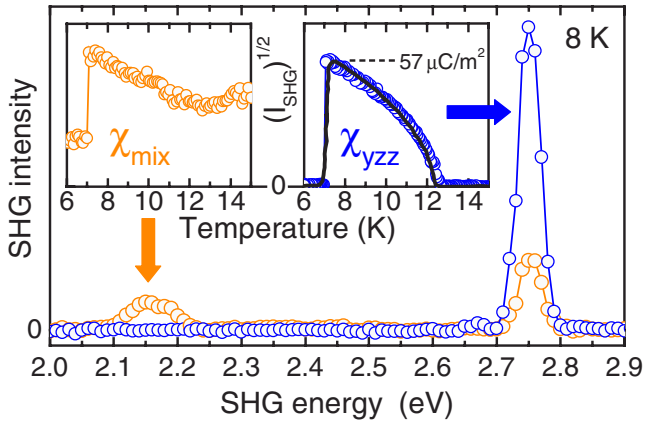

FIG. 1 (color online). Optical SHG on $MnWO_4$(100). The spectrum shows the SHG intensity I_{SHG} for the nonlinear susceptibilities χ_{yzz} and χ_{mix} (see text). Insets show the temperature dependence of $\sqrt{I_{\mathrm{SHG}}}$. The black solid line shows the spontaneous polarization adopted from Ref. [12].

Our assignment of SHG contributions is supported by Fig. 2, which shows the spatially resolved distribution of SHG light in the multiferroic phase. Figures 2(a) and 2(b) show SHG images gained at 2.75 eV from $(\chi_{\mathrm{FEL}} + \chi_{\mathrm{para}})$ and at 2.15 eV from $(\chi_{\mathrm{AFM}} + \chi_{\mathrm{para}})$. All images reveal differently shaded regions separated by abrupt changes of the SHG yield. These regions correspond to FEL $(\sim\chi_{\mathrm{FEL}} + \chi_{\mathrm{para}})$ and AFM $(\sim\chi_{\mathrm{AFM}} + \chi_{\mathrm{para}})$ domains. The different

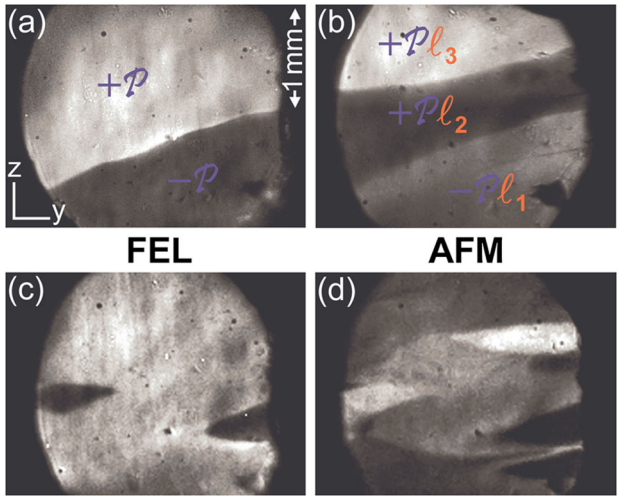

FIG. 2 (color online). Coexistence of FEL and AFM domains in zero-field-cooled $MnWO_4$(100). Images were obtained at 8 K with SHG at (a, c) 2.75 eV from $(\chi_{yzz} + \chi_{\mathrm{para}})$, and (b, d) 2.15 eV from $(\chi_{\mathrm{AFM}} + \chi_{\mathrm{para}})$. FEL and AFM domains are denoted by $\mathcal{P}$ and ℓ, respectively. Sets (a, b) and (c, d) were obtained in consecutive cooling cycles.

brightness is caused by the dependence of the amplitude and/or phase of the SHG contribution on the orientation of the order parameter and by the interference with the SHG contribution from χ_{para} [16,19]. The FEL domain structure reveals only two degrees of brightness. This is in agreement with the existence of two types ($\pm P_y$) of FEL domains. Although an electric polarization induced by magnetic order has by now been observed in a multitude of materials, Figs. 2(a) and 2(c) constitute the first observation of a domain structure for such a polarization. Along with the observation of a hysteresis (Fig. 3 and Ref. [20]) this confirms its ferroic nature.

Figure 2(b) shows the AFM domain structure coexisting with the FEL domain structure in Fig. 2(a). Three magnetic domains are distinguished by their brightness levels and labeled ℓ_{1-3}. The wall between domains ℓ_1 and ℓ_2 coincides with the FEL wall, which indicates that these magnetic domains possess an opposite chirality corresponding, as explained, to an opposite sign of P_y. However, the additional wall between domains ℓ_2 and ℓ_3 corroborates that for a given orientation of the FEL order parameter, different AFM 180° and rotation domains are possible. Although these translation domains possess the same chirality (and are thus indistinguishable by neutron diffraction), they are nevertheless distinguishable by SHG because of the phase shift of the SHG wave between different translation domains. A heating cycle through the paramagnetic phase leads to the more complex domain structures in Figs. 2(c) and 2(d). The two expected FEL domains are obtained, but they are accompanied by a much larger variety of magnetic domains. The FEL and AFM domain topologies are changed entirely by the heating cycle—domain-wall pinning effects are not observed. The lateral extension of the domains is in the range 0.1–1 mm, which is a typical value for spiral and nonspiral AFM structures [16,21]. Field-energy minimization effects in the FEL domain topology are not apparent, probably because of the small value of the FEL polarization.

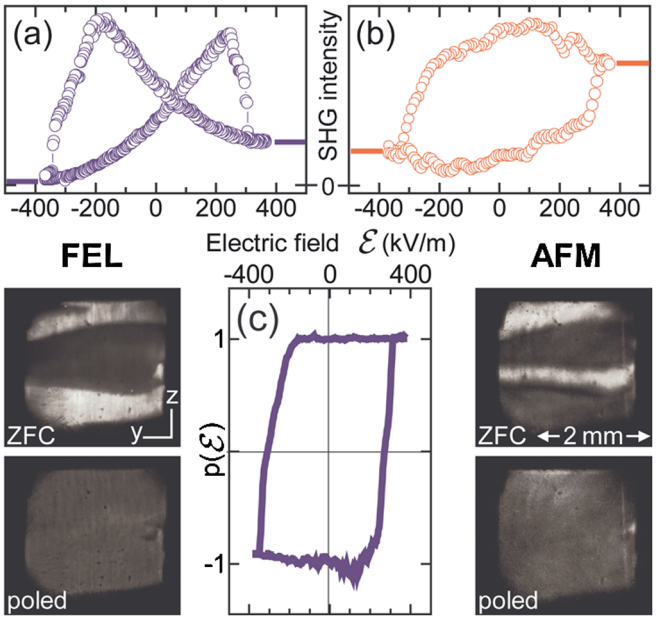

FIG. 3 (color online). Control of AFM domain structures by electric fields. (a, b) Intensity of "electric" and "magnetic" SHG in electric-field cycles with $\mathcal{E}||y$. Bars denote the end points of the hysteresis. (c) FEL hysteresis derived from (a) on the basis of Eq. (2). Images: FEL and AFM domain structures with SHG from ($\chi_{yzz} + \chi_{\text{para}}$) and ($\chi_{\text{AFM}} + \chi_{\text{para}}$), respectively, taken at 10 K after zero-field cooling (ZFC) and after subsequent poling in an electric field of 350 kV/m.

Figure 3 shows the response to a static electric field $\mathcal{E}||y$. For this purpose the sample was mounted between electrodes of 9×6 mm^2. In Figs. 3(a) and 3(b) the spatially integrated intensity of the SHG signals from ($\chi_{\text{FEL}} + \chi_{\text{para}}$) and ($\chi_{\text{AFM}} + \chi_{\text{para}}$), respectively, are shown for a field cycle in the ± 350 kV/m range. SHG images show the coexisting FEL and AFM domain structures obtained by zero-field cooling and by application of 350 kV/m subsequent to the zero-field cooling.

The butterfly loop in Fig. 3(a) clearly indicates the presence of a FEL hysteresis. The actual rectangular-shaped hysteresis $p(\mathcal{E})$ (with $-1 \leq p \leq +1$ as normalized FEL polarization and $p = \pm 1$ as saturation values) manifests as butterfly-shaped SHG intensity $I(2\omega)$ because of the interference with other SHG contributions:

$$I(2\omega) \propto |p(\mathcal{E})\chi_{\text{FEL}} + \chi_{\text{para}} e^{i\varphi} + \mathcal{E}\chi_{\text{EFISH}} e^{i\varphi'}|^2 |\vec{E}(\omega)|^4. \quad (2)$$

The three terms in Eq. (2) are the hysteresis-shaped FEL contribution (i), the paramagnetic background contribution (ii), and a contribution scaling with the applied electric field $\mathcal{E}$ and documented as "electric-field-induced second harmonic" (EFISH) in the literature [22] (iii). The phase shift between these SHG contributions is parametrized by the angles φ and φ'. By fitting Eq. (2) to the SHG data in Fig. 3(a) the actual rectangular-shaped hysteresis $p(\mathcal{E})$ is extracted and shown in Fig. 3(c). In agreement with dielectric measurements [20] the coercive field is about ± 280 kV/m. The hysteresis was confirmed by SHG images taken at various values of $\mathcal{E}$. Only where the polarization reversal progresses is a FEL multidomain structure observed. Outside these intervals the sample maintains a single-domain state.

Most remarkably, the AFM subsystem reproduces the hysteretic behavior of the FEL subsystem. As mentioned before, the spin chirality expressed by $k_{x,z}$ must reverse along with P_y so that by acting on the FEL domains with an electric field we "drag along" the magnetic chirality domains. However, this should leave the substructure of 180° and rotation domains within a chirality domain untouched. Yet SHG imaging reveals that the electric coercive field transforms the sample into a magnetic single-domain state. Figure 3(b) shows that repeated polarization reversal also switches the AFM order parameter repeatedly. The magnetic single-domain states encountered by this poling pro-

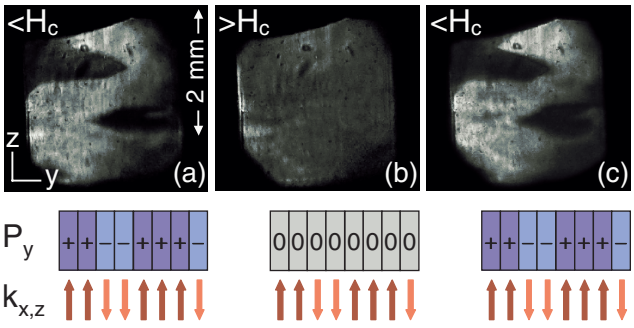

FIG. 4 (color online). Control of FEL domain structures by magnetic fields. (a) FEL domain structure of $MnWO_4(100)$ sample after zero-field cooling. (b) Application of a magnetic field $H_y > H_c$ with $H_c = 4.3$ T at 12 K quenches the magnetic spiral and, thus, the FEL order. SHG stems from χ_{para} only. (c) By returning to $H = 0$ the FEL order of (a) reemerges because the propagation vector as the source of the FEL polarization was not affected by the magnetic field. Sketches exemplify how the components $k_{x,z}$ of the magnetic propagation vector determine the FEL polarization P_y in (a) to (c). SHG images were taken with light from $(\chi_{\text{FEL}} + \chi_{\text{para}})$.

cedure are the same in each field cycle so that the SHG loop is always closed as seen in Fig. 3(b). (We speculate that although the volume-averaged magnetoelectric effect is canceled, local magnetoelectric effects, in particular, those acting on the low-symmetry domain walls, may lead to this preference.) Hence, the electric field fully controls the orientation of the magnetic order parameter so that Fig. 3(c) can be interpreted as FEL and also as AFM hysteresis. Note that the response of $BiFeO_3$ to an electric field is pronouncedly different [5]. In $BiFeO_3$ the ferroelectric order arises independent of the magnetic order so that an electric field, though manipulating the magnetic domain population, does not set a unique magnetic single-domain state.

While the electric field switches the magnetic order parameter of $MnWO_4$ in a controlled way, a magnetic field protects the FEL state against polarization reversal. This is demonstrated by Fig. 4 which shows the FEL domain structure of a $MnWO_4(100)$ sample in a magnetic field cycle. The FEL state in Fig. 4(a) is quenched when in a magnetic field along the y axis the boundary to the AF3 phase is crossed. In the high-field phase all spins are collinear, leading to $P_y = 0$ in Eq. (1) and SHG from χ_{para} only in Fig. 4(b). However, as known from neutron experiments [10], the magnetic propagation vector and, hence, the sign of $k_{x,z}$ remains unaffected by the field. Therefore, the FEL domain topology of Fig. 4(a) reemerges in Fig. 4(c) when the magnetic field is removed. The ferroelectrically stored information is "concealed" by the magnetic field, but its magnetic source is conserved and allows one to reconstruct the FEL state in a unique way.

In summary, we have spatially resolved the coexistence, coupling, and manipulation of AFM spiral domains and magnetically induced FEL domains in multiferroic $MnWO_4$. Two sets of magnetic chirality domains are uniquely coupled to two ferroelectric 180° domains, but since each set includes four possible types of magnetic 180° and rotation domains, the magnetic and electric domain structures retain a degree of independence. However, the magnetic domains are uniquely controlled by an electric field, and the poling behavior of the FEL domains is controlled by a magnetic field. The magnetic field quenches the spontaneous polarization but conserves its magnetic origin so that a ferroelectric domain state is reversibly hidden instead of irretrievably destroyed.

Regarding long-term application, a vastly increasing variety of spin-spiral compounds allowing ferroelectricity according to Eq. (1) is at our disposal for multifunctional magnetoelectric order-parameter control [8]. Systems with conical spin spirals suggest themselves for electric-field control of a macroscopic magnetization, and the discovery of mechanisms promoting magnetically induced ferroelectricity different from Eq. (1) is only a question of time and may even lead us towards high-temperature applications of magnetoelectric phase control.

The authors thank the DFG (SFB 608) for subsidy.

*fiebig@hiskp.uni-bonn.de

[1] W. Eerenstein, N. D. Mathur, and J. F. Scott, Nature (London) **442**, 759 (2006).
[2] M. Fiebig, J. Phys. D **38**, R123 (2005).
[3] E. Ascher *et al.*, J. Appl. Phys. **37**, 1404 (1966).
[4] T. Zhao *et al.*, Nature Mater. **5**, 823 (2006).
[5] S. Lee *et al.*, Phys. Rev. B **78**, 100101(R) (2008).
[6] N. Hur *et al.*, Nature (London) **429**, 392 (2004).
[7] P. G. Radaelli *et al.*, Phys. Rev. Lett. **101**, 067205 (2008).
[8] T. Kimura, Annu. Rev. Mater. Res. **37**, 387 (2007).
[9] M. Mostovoy, Phys. Rev. Lett. **96**, 067601 (2006).
[10] G. Lautenschläger *et al.*, Phys. Rev. B **48**, 6087 (1993).
[11] K. Taniguchi *et al.*, Phys. Rev. Lett. **97**, 097203 (2006).
[12] A. H. Arkenbout *et al.*, Phys. Rev. B **74**, 184431 (2006).
[13] J. Rossat-Mignod, in *Methods of Experimental Physics*, edited by K. Skold and D. L. Price (Academic, New York, 1987), Vol. 23C, p. 69.
[14] H. Sagayama *et al.*, Phys. Rev. B **77**, 220407(R) (2008).
[15] *Nonlinear Optics in Metals*, edited by K. H. Bennemann (Clarendon Press, Oxford, 1998).
[16] M. Fiebig, V. V. Pavlov, and R. V. Pisarev, J. Opt. Soc. Am. B **22**, 96 (2005).
[17] M. Fiebig *et al.*, Nature (London) **419**, 818 (2002).
[18] R. R. Birss, *Symmetry and Magnetism* (North-Holland, Amsterdam, 1966).
[19] In the case of the FEL domains χ_{para} was admixed by rotating the $MnWO_4(100)$ sample by $\sim 10°$ around z.
[20] B. Kundys, C. Simon, and C. Martin, Phys. Rev. B **77**, 172402 (2008).
[21] P. D. Evans *et al.*, Science **295**, 1042 (2002).
[22] C. H. Lee, R. K. Chang, and N. Bloembergen, Phys. Rev. Lett. **18**, 167 (1967).